Simultaneous Determination of Size and Shape of Single α-Synuclein Oligomers in Solution

Saurabh Awasthi[1*], Cuifeng Ying[1], Jiali Li[2], Michael Mayer[1*]

[1] Adolphe Merkle Institute, University of Fribourg, Chemin des Verdiers 4, CH-1700 Fribourg, Switzerland

[2] University of Arkansas, Fayetteville, AR, United States

*Corresponding Author Email ID: saurabh.awasthi@unifr.ch, michael.mayer@unifr.ch

Keywords: Amyloid oligomers, α-synuclein, aggregation, nanopore, resistive-pulse sensing

Abstract

Soluble oligomers of amyloid-forming proteins are implicated as toxic species in the context of several neurodegenerative diseases. Since the size and shape of oligomers influences their toxicity, their biophysical characterization is essential for a better understanding of the structure-toxicity relationship. Amyloid oligomers are difficult to characterize by conventional approaches due to their heterogeneity in size and shape, their dynamic aggregation process, and their low abundance. This paper demonstrates that resistive-pulse measurements using polymer-coated solid-state nanopores enable label-free characterization of αSynuclein oligomers with single-particle resolution. This approach determines the size and shape of individual oligomers in solution and it interrogates hundreds of particles within minutes. A comparison of the resulting size distribution with single-particle analysis by transmission electron microscopy and mass photometry reveals good agreement and superior resolution. In addition, nanopore-based analysis is attractive due to its unique capability to combine rapid size analysis with an approximation of oligomer shape. Applying this shape

approximation to putatively toxic oligomeric species that range in concentration from picomolar to nanomolar and in size from 11-25 mer (10S) and 19-39 mer (15S), revealed shapes that agree well with previous estimates by cryo-EM with the advantage that nanopore-based analysis occurs rapidly, in solution, and has the potential to become a widely accessible analysis technique.

Introduction

Neurodegenerative diseases characterized by misfolding and aggregation of α-synuclein (αSyn) protein (14.5 kDa) are collectively termed synucleinopathies.[1-4] The most common types of synucleinopathies are Parkinson's disease (PD), dementia with Lewy bodies (DLB), and multiple system atrophy (MSA).[3] Oligomers of αSyn are neurotoxic species and implicated in the pathology of Parkinson's disease.[5-9] Colla et al. showed that αSyn accumulates within the endoplasmic reticulum or in microsomes forming toxic oligomers in transgenic mouse brain leading to α-synucleinopathy.[10] Prots *et al.* demonstrated that αSyn oligomers disrupt axonal integrity in human neurons and that increased αSyn oligomerization by expressing oligomer-forming mutants (E46K and E57K) of αSyn resulted in impaired axonal transport of mitochondria.[11]

Although most soluble oligomeric species of αSyn are toxic,[9] the molecular basis of toxicity remains to be established.[12] Therefore, the biophysical characterization of αSyn oligomers is essential for understanding their pathology and developing therapeutic interventions. Characterization and quantification of αSyn oligomers, however, remains challenging with established approaches due to the heterogeneity of oligomeric species with regard to their size, shape and their low abundance with concentrations ranging from picomolar (pM; 10^{-12} mol l^{-1}) to nanomolar (nM; 10^{-9} mol l^{-1}).[13, 14] One reported mechanism of toxicity of αSyn oligomers is the interactions with lipids and formation of pore in phospholipid membranes.[15-17] The physical properties of αSyn oligomers such as oligomer size or conformation/shape are key determinants of their pore-forming activity and toxicity.[17-21] Only

specific sizes (i.e., oligomers with a certain number of monomers) or specific shapes (such as annular or disc-shaped) oligomers have exhibited neurotoxicity in vivo. [9, 17, 20] Recently, Kiechle et al. used in vivo protein complementation to identify presynaptic oligomerization and age-dependent accumulation of potentially toxic αSyn oligomers in a specific size range (8-16-mer).[22] Also, prior work has demonstrated neurotoxic αSyn oligomers composed of ~30 monomers,[23] >30 monomers and 10-40 monomers.[20, 24] Methods based on ensemble analysis, such as size exclusion chromatography (SEC), analytical ultracentrifugation (AUC), small-angle X-ray scattering (SAXS), dynamic light scattering (DLS), and gel electrophoresis, fail to capture the entire range of heterogeneity in size with good resolution and they either cannot determine oligomer shape or struggle to do so in heterogenous mixtures. In addition, the need for fluorophore labeling, cross-linking or preparation of dry samples of some existing methods may result in undesirable alterations in the physical and biochemical properties of amyloid oligomers.[25, 26] Recently, Arter et al. used microfluidic free-flow electrophoresis as a solution-based approach to fractionate stable αSyn oligomer ensembles for achieving structural, kinetic and immunological characterization in addition to the measurement of oligomer ζ-potential of each fraction.[27] Alternative, ensemble-based attempts have employed fluorescence methods such as single-molecule Förster resonance energy transfer (smFRET),[21] and single-molecule photobleaching to characterize αSyn oligomers in vitro for oligomer size analysis.[28] The goal of the work presented here was to address the analytical challenge of oligomer heterogeneity by establishing an accessible and practical method for characterization of αSyn oligomers on a single oligomer level, rapidly, and in solution.

An elevated level of αSyn oligomers in cerebrospinal fluid (CSF) or plasma is associated with the onset and progression of neurodegenerative synucleinopathies,[29, 30] therefore, αSyn oligomers are promising biomarker candidates. Commonly used immunoassays to quantify amyloid oligomers such as enzyme-linked immunosorbent assay (ELISA),[31, 32] single-molecule array (SIMOA) assays[33, 34]

and surface-based fluorescence intensity distribution analysis (sFIDA)[35] require the use of high-affinity antibodies and typically fail to discriminate oligomers from monomers and fibrils. Moreover, a recent study by Kumar et al. tested sixteen so-called "conformation-specific αSyn antibodies," and none of these antibodies showed specificity for any particular aggregate size of αSyn.[33] Given the current challenges associated with immunological assays for oligomer quantification, an urgent need exists for an antibody-free, sensitive approach that can determine oligomer size, abundance and ideally conformation/shape. We suggest that one attractive approach to address this need may be to monitor aggregation using nanopores.[36-44] So far most studies using nanopores focused on either detecting protein aggregates or on following the aggregation process over time.[37, 39, 44] For instance, we have used nanopores to characterize amyloid-β (Aβ-40 and Aβ-42) aggregates to differentiate different aggregates including oligomers, protofibrils, and fibrils.[45] Also, in another study using Aβ-40 and Aβ-42, we showed that for both peptides, the abundance of oligomers in the 4-mer to 13-mer range correlated with both pore formation and cytotoxicity, while monomers, dimers, trimers, and the largest oligomers (>210 kDa) were negatively correlated to both phenomena.[46] Beyond characterizing the size and shape of proteins and protein aggregates, we have used lipid-bilayer and polymer-coated solid-state nanopores to fingerprint individual protein molecules and protein complexes by determining their size, shape, charge, rotational diffusion coefficient, and dipole moment of individual proteins.[47-50]

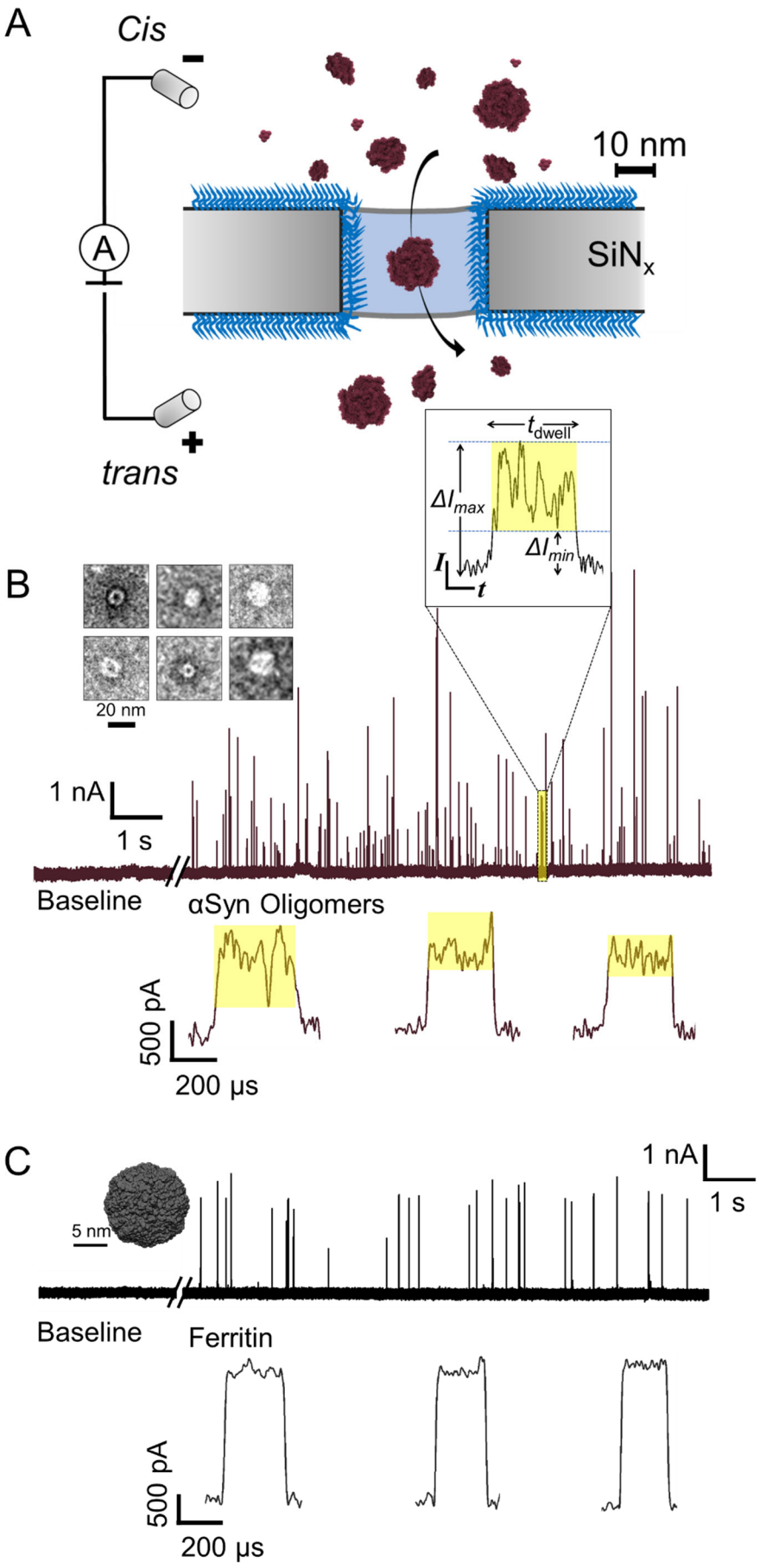
A
Cis
10 nm
SiNx
trans
B
20 nm
1 nA
1 s
Baseline
αSyn Oligomers
500 pA
200 µs
C
5 nm
1 nA
1 s
Baseline
Ferritin
500 pA
200 µs

Figure 1. Nanopore-based, single-particle characterization of α-synuclein oligomers in solution. A. Schematic illustration of the experimental setup to measure resistive pulses due to the translocation of individual αSyn oligomers through a polymer coated (blue) nanopore. **B.** Original current recordings before and after adding αSyn oligomers show resistive pulses due to the translocation of αSyn oligomers as upward spikes. The TEM image in the inset shows individual αSyn oligomers from the sample used for nanopore experiments. Characteristic translocation events from the passage of individual αSyn oligomers through the nanopore illustrate the dwell time (t_d), minimum current blockade (ΔI_{min}), and maximum current blockade (ΔI_{max}) that arise from the rotational dynamics as non-spherical oligomers move through the electric field inside the nanopore. The magnitude of current blockade ΔI is proportional to the particle volume, while the intra-event current modulations (shaded in yellow) contain information about the size and shape (m) of each oligomer in solution.[47, 48] Three additional examples of translocation events (t_d >150 µs) from the passage of individual αSyn oligomers through a nanopore are shown below. **C**. Original current recordings before and after adding the perfectly spherical protein ferritin (PDB ID: 6TSF), show resistive pulses as upward spikes due to single protein translocations. Note that the three examples of translocation events that are shown in detail (t_d >150 µs) from the passage of ferritin through the same nanopore result in square-shaped resistive pulses with small intra-event current modulations. For this work we used nanopores that resulted in such square-shaped resistive pulses for ferritin translocations, indicating that these pores correctly indicate small current modulations from rotations of a perfectly spherical protein as expected and as reported before.[47, 48]

The work presented here, demonstrates that resistive pulse sensing with solid-state nanopores makes it possible to estimate the size and shape of single αSyn oligomers. This approach enables classification of each Syn oligomer into small (2-5 monomers), medium (5-15 monomers), and large (>15 monomers) species, depending on the number of monomers in each aggregate. In addition, current modulations caused by rotation of single oligomers as they translocate through a uniform electric field inside a nanopore make it possible to estimate the ellipsoidal shape of individual oligomers in terms of their length-to-diameter ratio (m). This shape analysis reveals oligomer populations with different shape corresponding to a disc, prolate and spherical shape. Also, the size and shape analysis of individual oligomers makes it possible to identify so-called "toxic oligomers" of specific sizes such as 10S and 15S[20] and specific shapes such as wreath-shaped, or tubular-shaped

annular oligomers, which have been reported to possess pore-forming properties and toxicity.[21] Moreover, the frequency of translocations reveals the concentration of αSyn oligomers of various sizes and shapes.

Results and Discussion

Analysis of the size of α-synuclein oligomers at the single-particle level

Figure 1A illustrates the experimental setup for resistive pulse measurements using solid-state nanopores. A single pore with a diameter of 26 nm to 56 nm in a thin insulating silicon nitride (SiN_x) membrane separates two compartments containing electrolytes. A high-gain, low-noise patch-clamp amplifier applies a potential difference (±0.1 V) between these compartments and monitors the ionic current through the nanopore. Passage of individual αSyn oligomers through the nanopore displaces conducting electrolyte, resulting in characteristic resistive pulses. These resistive pulses contain information about the physical properties of the translocating particles, including their volume (i.e., size 'Λ') and shape (i.e., length-to-diameter ratio 'm') (**see Figure 1B**).[47] The dwell time that a protein resides in the pore, t_d, is influenced by its electrophoretic mobility and hence its net charge. In addition, the frequency of observed translocation events is proportional to the concentration of oligomers.[51]

Figure 1B shows original current traces of electrical recordings through nanopores, featuring translocation events of individual oligomers as resistive upward spikes (i.e. reductions in the amplitude of the negative baseline current). In order to evaluate the benefits of nanopore-based oligomer characterization on the single particle level, we employed pre-characterized samples of αSyn oligomers obtained from ND Biosciences, Switzerland and prepared as explained by Kumar et al.[52] To determine the size distribution of these samples, we recorded thousands of individual

translocation events of αSyn oligomers. We classified αSyn oligomers based on their size in terms of the number of monomers they contain. To this end, we used the volume of monomeric αSyn protein, which we estimated to be 35 nm^3 using nanopore experiments (**See Supplementary Note 1 and Supplementary Figure S1**), which agrees well with earlier reports of αSyn monomer volume (~30 nm^3) determined by SAXS.[53] Oligomer sizes estimated by nanopores range from a dimer up to large-sized oligomers consisting of ~150 monomers, again in good agreement with the sizes of αSyn oligomers reported earlier.[20, 21, 54] **Figure 2A** shows that single-oligomer analysis of these samples using nanopores, revealed 10 maxima in the size distribution corresponding to 10 different sizes of the oligomer populations. We labeled different-sized oligomer populations as O^1 to O^{10} with increasing numbers of monomers. We confirmed the oligomer size estimates from the nanopore experiments with established single-particle methods, including negative staining TEM imaging (**Figure 2B**) and Mass Photometry (**Figure 2C**). Mass photometry is a recently introduced light-scattering-based method that also enables oligomer mass analysis at the single-particle level while they interact with a surface.[55, 56] The different oligomer populations determined by TEM (21-133 mer) and mass photometry (3-103 mer) agree well with the estimates by nanopore (4 mer-122 mer). Nanopore-based analysis revealed two small-sized oligomer populations, called as O^1 and O^2, corresponding to 4-mer (±2) and 8-mer (±5), which were also detected by mass photometry. Using TEM imaging, it was, however, difficult to detect these small-sized oligomers. Comparing oligomer size estimations using nanopores to those using TEM and mass photometry shows the agreement between the range of estimated sizes from all three methods and illustrates that the resolution to distinguish between differently sized oligomers is highest from nanopore experiments, which reveals 10 sub-populations in size, while the resolution of TEM imaging and mass photometry are limited to approximately half the number of sub-populations in size.

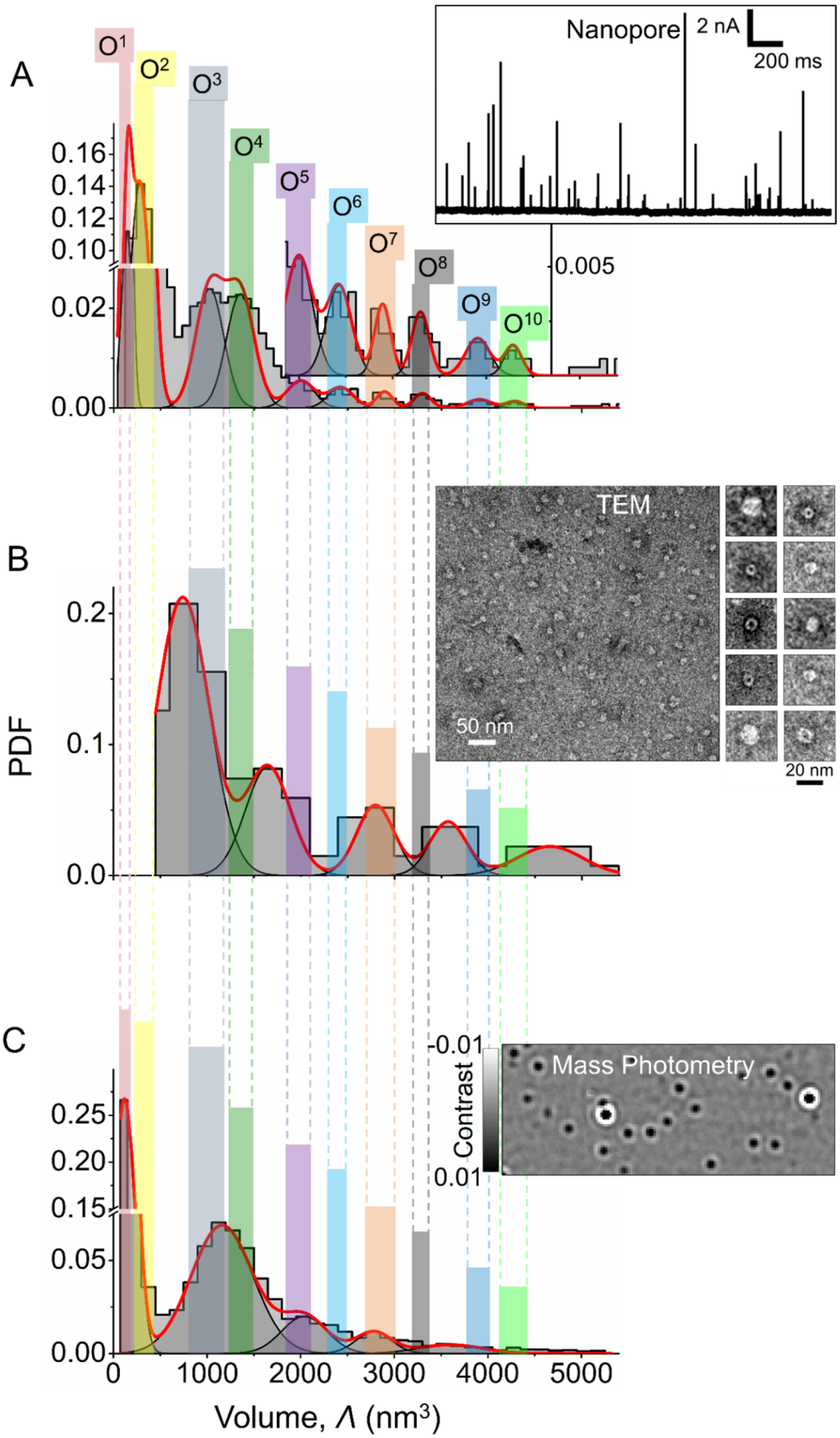

Figure. 2 Nanopores enable high-resolution analysis of oligomer size. A. Size distribution of αSyn oligomers as determined by nanopores. Differently-sized oligomer sub-populations identified using the nanopore-based

approach are marked as O^1 to O^{10} and range in size from a 4 (±3)-mer to 122 (±5)-mer. The inset shows original current recordings through a nanopore with resistive pulses due to the translocation of single αSyn oligomers as upward spikes. **B.** Size distribution of αSyn oligomers determined by TEM. The inset shows a TEM micrograph of αSyn oligomers used for the analysis. **C.** Size distribution of αSyn oligomers determined by single-particle mass analysis using mass photometry. The inset shows a differential interferometric scattering image of αSyn oligomers. For comparison, the shaded regions in different colors show the presence/absence of different oligomer populations identified by nanopores, TEM, and mass photometry. Mass photometry is calibrated to reveal the molecular weight of each particle, we converted the molecular weight to particle volume using the molecular weight of αSyn monomers and assuming a monomer volume of 35 nm^3.

In addition, we compared the size distribution of αSyn oligomers obtained by nanopore recordings with previously reported sizes of αSyn oligomers. One of the major oligomer populations identified by nanopores labeled as O^2 consisting of 2-14 monomers, agrees well with αSyn oligomers containing 8-16 monomers recently reported to accumulate in the brain of transgenic mouse models with increasing age as determined by protein complementation approach.[22] Two other major αSyn oligomer populations labeled as O^3 and O^4 consisting of ~30 and ~39 monomers, agree well with earlier reports of ~30-mer αSyn oligomers as determined by size exclusion chromatography (SEC) coupled with multiangle laser light scattering (MALLS),[23] SAXS,[57] analytical ultracentrifugation (AUC),[58] and single-molecule photobleaching experiments.[28] We confirmed the presence of these αSyn oligomer populations, labelled as O^3 and O^4, by particle size analysis using TEM and mass photometry and highlighted them with light blue and light green shaded regions in **Figure 2B, 2C**. While mass photometry made it possible to identify small-sized oligomers such as 4-mers, its resolution was limited to five different oligomer sizes. We also used TEM for particle size analysis to determine oligomer size distribution but it could not detect small oligomers (such as 4-mer and 8-mer). Overall, the peaks in the size distribution from all three methods indicate that certain sizes of αSyn oligomers are more probable in the sample than others. Among these preferred sizes are

oligomers composed of 4 (±3) monomer (O^1, **Figure 2A, C**), 11 (±3) monomers (O^2, **Figure 2A, C**), 25 ± 10 monomers (O^3, **Figure 2A, B, C**), 44 (±4) monomers (O^4, **Figure 2 A, B, C**), 57 (±8) monomers (O^5, **Figure 2A, B, C**).

Analysis of the shape of individual αSyn oligomers

To determine the shape of αSyn oligomers, we analysed the current modulations during individual translocation events of single oligomers through nanopore. Nanopore-based resistive pulse recording makes it possible to approximate the spheroidal shapes of individual particles translocating through the pore.[47] This approximation models particle shape with an ellipsoid spheroid of the same volume and returns the ratio, *m* between the short and the long axis of the ellipsoid that best represents each individual αSyn oligomer.[48] To this end, nanopore-based shape analysis exploits the ΔI_{min} and ΔI_{max} values (**Figure. 1B**), which correspond to the two extreme orientations of a non-spherical particle with certain volume and shape in the electric field of the nanopore. Earlier studies examining the morphology of αSyn oligomers based on TEM, atomic force microscopy (AFM), and small angle x-ray scattering (SAXS) have revealed oligomers with spherical,[59, 60] annular, toroidal, flattened disc-like, globular and prolate shapes.[20, 23, 53, 61, 62] Here, based on the ΔI_{min} and ΔI_{max} values of each translocation event, we model the shape of each oligomer in one attempt as an oblate ellipsoid and in the other attempt as a prolate ellipsoid since solutions for both models can be found for many particles. TEM imaging of the same samples revealed the absence of any large size fibrillar or elongated aggregates that may exceed the length of the nanopore (**Figure 2B**), making it possible to use the same analysis of volume-exclusion in the nanopore for characterizing all translocation events. In addition, we confirmed that nanopore recording at the high ionic strength (i.e., 2 M KCl) that we used, does not change the αSyn oligomer size distribution during the experiment compared

to solutions with physiologic ionic strength (**Supplementary Note 2, Supplementary Figure S2** and **S3**).

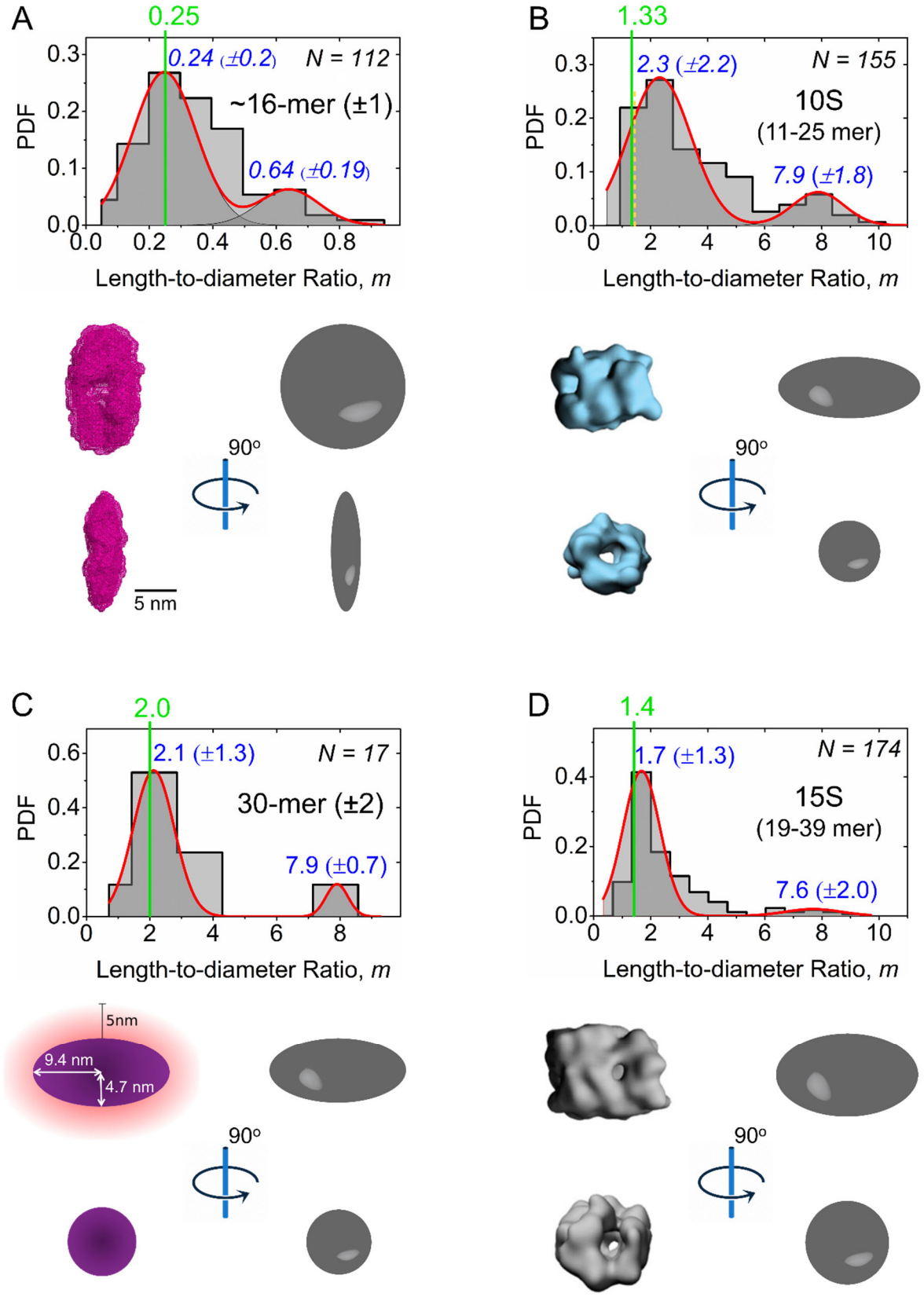

Figure. 3 Shape approximation of toxic αSyn oligomers in solution. A. Histogram of the length-to-diameter ratio, *m* of oligomers consisting of 15-17 αSyn monomers. The cartoon below shows a comparison of the approximated ellipsoidal shape of a ~16-mer as determined by nanopore (as grey spheroids) with the structure of the 16-mer (mesh representation, in pink) as revealed by SAXS experiments, adopted with permission from Ref [53] **B**. Histogram of the length-to-diameter ratio of 10S oligomers consisting of 11-25 αSyn monomers. The cartoon below shows a comparison of the approximated ellipsoidal shape as determined by nanopore (as grey spheroids) with the known three-dimensional structures for 10S oligomers determined by cryo-EM, reprinted with permission from REF [20]. The dashed line in yellow marking the first bin of the histogram, which represents the second most probable bin of the shape distribution for this oligomer size range (11-25 monomers) as determined by nanopore experiments shows excellent agreement with the previously reported[20] shape value (green line). **C**. Histogram for the length-to-diameter ratio of 30 (±2)-mer oligomers. The cartoon below shows a comparison of the approximate ellipsoidal shape of 30-mers as determined by nanopore (as grey spheroids) with ellipsoidal model of the 30-mer determined by SAXS, reprinted with permission from REF [23] **D**. Histogram of the length-to-diameter ratio of 15S[20] oligomers consisting of 19-39 αSyn monomers. Comparison of the approximate ellipsoidal shape as determined by nanopore (as grey spheroids) with the known three-dimensional structures for 15S oligomers determined by cryo-EM, reprinted with permission from REF [20]. The most probable *m* value of each population is shown at the top in blue. The solid lines in light green show the reference length-to-diameter ratio, *m*, for the respective oligomeric species.

Simultaneous determination of oligomer size and shape of each particle provides opportunity to analyse oligomer sub-populations with respect to their size and shape. For instance, we determined the shape of αSyn oligomers in a size range that was previously described to include toxic oligomers (**See Figure 3A-D**). Giehm et al. determined a wreath shape with length-to-diameter ratio, *m* of 0.25 of so called "vesicle disrupting α-synuclein oligomers" consisting of ~16 monomers.[53] **Figure 3A** shows the distribution of *m* values obtained for the prolate model of 16-mer (±1) oligomers by nanopore experiments and reveals that the major oligomer population corresponds to an oblate shape value of *m* = 0.24 in excellent agreement with the reported shape of 0.25 from SAXS experiments.[53] In addition to this dominant sub-population, nanopore-recordings identified a second

sub-population with a shape value of *m* = 0.64 in the same sample. Due to its low abundance, this sub-population may not be detectable in SAXS-based ensemble analysis.

Figure 3B and **3D** show the distribution of the approximated shape of so-called "kinetically trapped toxic αSynuclein oligomers" with two sizes: 10S (11-25 mer) and 15S (19-39 mer), which were characterized as prolates with *m* values of 2.0 for 10 S oligomers and 1.4 for 15S oligomers based on their sedimentation coefficients.[20] We observed a dominant oligomer population with a length-to-diameter ratio, *m* of 2.3 for the 10S oligomers and a major oligomer population with a length-to-diameter ratio, *m* of 1.7 for the 15S oligomer in close agreement with these previously reported[20] shape values.

In addition to these studies, Lorenzen et al. used size exclusion chromatography in combination with multiangle scattering and SAXS and determined a prolate ellipsoid shape with a *m* value of 2.0 for oligomers consisting of ~30 monomers (±2).[23] The nanopore experiments carried out here indicate a major population with a *m* value of 2.1 in the distribution of the length-to-diameter ratio of 30-mer oligomers (**Figure 3C**), in excellent agreement with the reported shape value of 2.0. Overall, **Figure 3** indicates that for oligomeric species within size brackets that have previously been reported as toxic, nanopore recordings resolve typically two distinct sub-populations in oligomer shape as a result of shape analysis of each oligomer particle one by one.

Quantifying αSyn oligomers

In order to assess if nanopore-based analysis is able to quantify the total concentrations of αSyn oligomers as well as the concentration of sub-populations, we monitored the frequency of individual translocation events through nanopores at increasing oligomer concentrations ranging from

picomolar (pM; 10^{-12} mol l^{-1}) to nanomolar (nM; 10^{-9} mol l^{-1}). **Figure 4A** shows that the frequency of translocation events increased linearly with increasing total oligomer concentration. **Figure 4B** shows that the translocation event frequency is directly proportional to the total concentration of αSyn oligomers at least up to ~2.5 nM (**See Figure 4B**). This ability is beneficial for assessment of the αSyn oligomers concentration as a potential biomarker for PD. PD biomarker analysis will benefit from the ability to count individual oligomer translocations using the nanopore-based method because is not limited to quantifying the total concentration of oligomers but makes it possible to identify and quantify the fraction of sub-populations. For instance, it can determine the concentration of αSyn oligomers of certain sizes such as 8-10 mers, 21-39 mers, 40-50 mers, which are considered toxic. Or it can quantify the fraction of oligomers with a certain shape or the combination of a certain size and shape as a direct consequence of the characterization of each translocation event with respect to the size and shape of the oligomer particle that caused it combined with its measured frequency of occurrence.

This analysis, therefore, provides proof of principle for nanopore-based characterization and quantification of amyloid oligomers at the single-oligomer level, in a heterogeneous mixture. In-solution measurements ensure minimal perturbation of the inherent biophysical properties of these aggregates with the possibility of simultaneous oligomer size and shape analysis. The nanopore-based approach allows counting of individual translocation events due to the passage of different size and shape oligomers in solution. In addition, the recent development of hydrogel interfaced nanopores combined with asymmetric salt concentrations may enable quantification of femtomolar particle concentrations (fM),[63] which would be excellent for biomarker analysis.

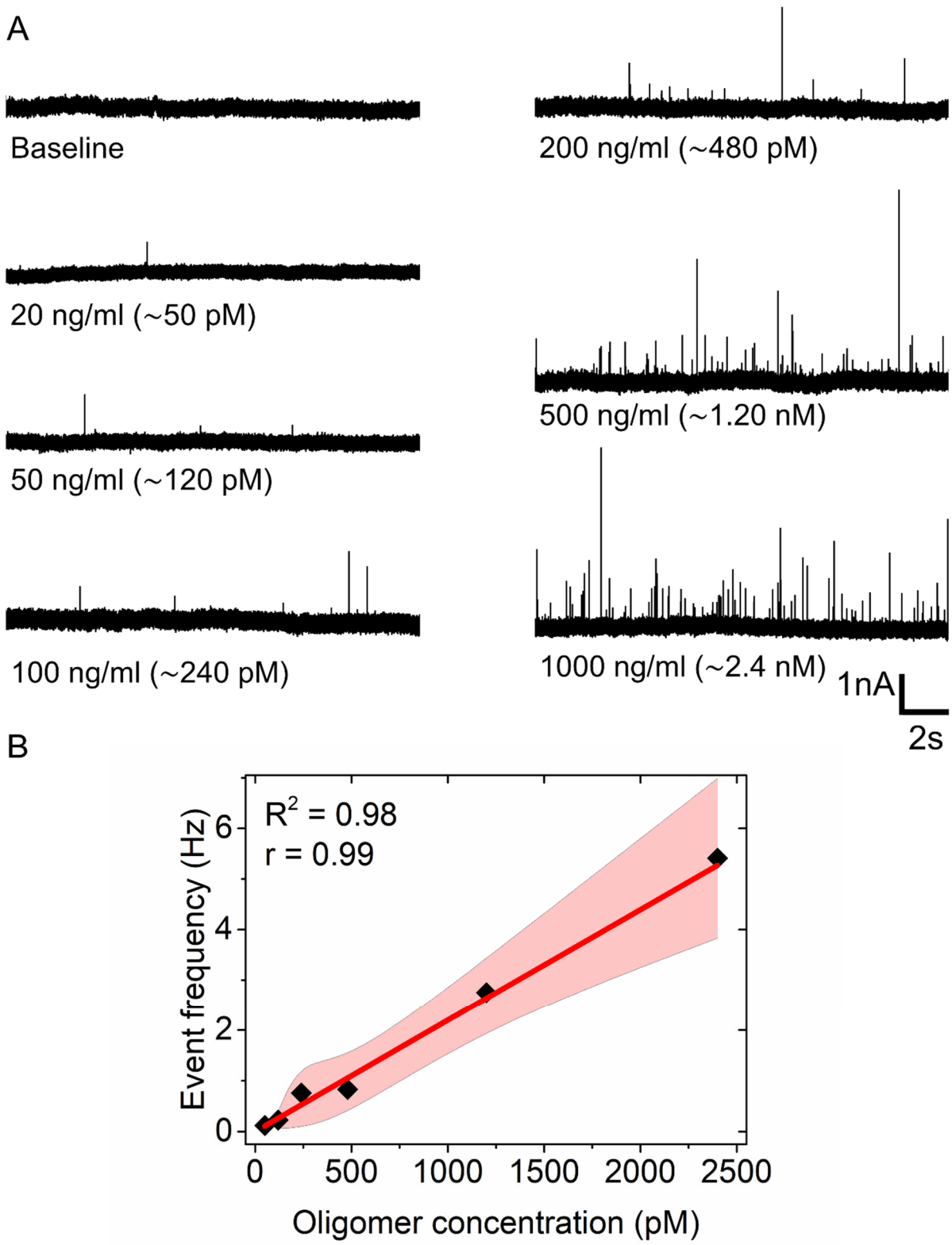

Figure. 4 Quantification of the abundance of αSyn oligomers using nanopores. A. Original current recordings (~20 seconds) low-pass filtered with a cut-off frequency of 57 kHz showing resistive pulses (as upward spikes) due to translocation of individual αSyn oligomers at increasing total concentrations ranging from 50 pM to 2.4 nM. **B.** Translocation event frequency at different oligomer concentrations. Translocation event frequency is

plotted as diamonds (in black) and the red solid line is a linear fit (slope of 0.002 and Pearson's r of 0.99). The shaded region (in light red) shows the standard deviation of four different measurements using a different nanopore chip for each measurement.

Conclusions

The work presented here demonstrates that nanopore-based characterization of αSyn oligomers can overcome some of the current challenges in oligomer characterization using conventional methods by providing (i) analysis of the size and shape of oligomers simultaneously, (ii) analysis of oligomers on a single-particle level, thereby circumventing the complications from the heterogeneity of sizes, (iii) measurements in solution and in a label-free manner, thereby examining oligomers in their native hydrated state, (iv) quantification of oligomer concentrations of total oligomer content or of specific sub-populations in size and, or shape that may be particularly toxic or diagnostically relevant. Since oligomers are considered to represent the key neurotoxic species,[8, 9, 20] a quantitative understanding of their abundance, physical property (i.e., size and shape) and heterogeneity in solution is essential to elucidate their structure-toxicity relationship. The nanopore-based approach presented here enables single-oligomer level, real-time size and shape estimation with minimal sample perturbation, in a heterogenous mixture, without the need for purification and it characterized oligomer samples within tens of minutes based on hundreds of translocation events; even at a low total oligomer concentration of 100 pM more than 100 translocation events are recorded within 10 minutes of total analysis time.

Determination of size-distributions by the nanopore-based approach revealed 10 differently-sized, stable sub-populations of oligomers as well as approximations of their shape on a single-particle level. This size resolution is two times higher than the one of mass photometry and TEM analysis. In addition, TEM-based characterization of oligomers and its potential use for biomarker

analysis is expensive, may involve dry-state sample preparation, and typically not available in clinical settings. Importantly these established single-particle methods do not have the capability to determine the shape of individual oligomeric species. Although the nanopore-based approach presented here currently requires specialized training and expertise, it has the potential to provide rapid, quantitative, label-free, and cost-effective multiparametric characterization of heterogeneous amyloid oligomers in solution. These benefits may address the urgent need for methods that make it possible to quantify amyloid oligomers as biomarkers or for testing drug targets to treat neurodegenerative disorders.[34, 64, 65]

Experimental

Materials

Oligomers of α-Synuclein were obtained from ND BioSciences, Switzerland as a part of a collaboration supported by the Michael J. Fox Foundation (MJFF-009813) MJFF. The preparation of αSyn oligomers has been discussed in detail by Kumar et al.[52] Oligomers of αSyn from ND Biosciences were aliquoted, flash frozen, and stored at the -80° C upon arrival and only taken out before the measurements. We obtained the EM-Tec Formvar Carbon support film on copper 200 square mesh (Cat. no. 22-1MFC20-100) for TEM imaging of αSyn oligomers from the company Micro to Nano, Netherlands. All the nanopores used in this work were purchased (pre-fabricated by Helium Ion Milling) from Norcada Inc., Canada or fabricated by helium ion beam sculpting, as explained previously at the University of Arkansas, USA.[66] The pre-fabricated nanopore chips (4x4 mm) obtained from Norcada contained 10x10 µm SiN_x window with a 30 nm thick SiN_x membrane and a 100 nm thick SiO_2 underlayer. We purchased all other chemicals and buffers from Sigma-Aldrich unless otherwise stated.

Resistive pulse sensing using nanopores

We carried out all resistive pulse sensing experiments using a recording buffer containing 2 M KCl, and 10 mM HEPES buffer (pH 7.4) as described earlier by Yusko et al.[47] and Houghtaling et al.[48] We used polymer-coated solid-state nanopores of 25 nm to 56 nm diameter to characterize αSyn oligomers in free translocation mode as described earlier.[48] We applied a constant potential of ±100 mV across the nanopore and then measured the current at a sampling rate of 500 kHz via USB-6361 using an AxoPatch 200B patch-clamp amplifier (Molecular Devices) in voltage-clamp mode (β = 1) in combination with LabVIEW (National Instruments) software. We filtered the acquired data with a Gaussian low-pass filter at a cut-off frequency of 50 kHz. We performed a threshold-search (5× the standard deviation of the baseline current) for resistive pulses within the current recordings and determined the oligomer size (as volume) and shape (as length-to-diameter ratio, *m*) by so called "intra-event analysis" as described earlier.[47, 48] For the analysis of shape with the previously described convolution algorithm,[47, 48] we constrained the spread "σ" the standard deviation of the current trace value to be greater than, or equal to, the standard deviation of baseline noise. We used Ferritin, a perfectly spherical protein, as a standard to identify the best nanopores, which accurately estimate the size and shape of ferritin and could then be used to determine the size and shape of Syn oligomers (**See Figure 1C**). During the size and shape analysis of Syn oligomers, we used nanopores that give a spherical shape value for Ferritin (with *m* value close to 1).

Transmission electron microscopy

Carbon coated 300-mesh copper grids (Electron Microscopy Sciences, Hatfield) were plasma cleaned for 5 s using an oxygen plasma cleaner (Zepto RIE, Dienner), before pipetting 5 µl of Syn oligomers sample (~100 µg/ml concentration) in PBS buffer, pH 7.4 on top of the grids followed by 2 min

incubation. The grids were washed in a water droplet. Uranyl acetate (2% w/v) was added (3 µl) and incubated for 2 min. Excess stain was blotted off with a filter paper and dried. TEM images were recorded with a FEI Tecnai Spirit operating at 120 kV. We used ImageJ for particle size analysis of Syn oligomers.[67]

Mass Photometry

We acquired all the mass photometry data using a TwoMP mass photometer (Refeyn Ltd, Oxford, UK) similar to that described previously by Sonn-Segev et al. with slight modifications.[55] Briefly, microscope coverslips (24 × 50 mm Thorlabs, Cat. No. CG15KH1) cleaned using isopropanol followed by pure water thrice sequentially were used along with PDMS CultureWell™ gaskets (Cat. No. GBL103250) for single-oligomer mass analysis. We diluted αSyn oligomers up to a concentration of ~250 ng/ml in PBS or in 2 M KCl immediately prior to mass photometry measurements. To determine the effect of ionic strength, αSyn oligomers were incubated for 90 min or overnight in PBS or 2 M KCl at room temperature. For each mass photometry acquisition, 20 µL of diluted protein was introduced into the flow chamber, and following autofocus stabilization, movies of 180 s duration were recorded. Each sample was measured at least three times independently ($n \geq 3$). Mass photometry data acquisition was performed using AcquireMP (Refeyn Ltd, v2.4.1). All mass photometry images were processed and analyzed using DiscoverMP (Refeyn Ltd, v2.5.0).

Acknowledgements

SA acknowledges financial supported by the Swiss National Science Foundation “SPARK” funding (CRSK-3_195960). MM acknowledges financial support from the Swiss National Science Foundation

(Grant number: 200020_197239), Michael J. Fox Foundation (MJFF-009813) and from the Adolphe Merkle Foundation, Switzerland.

References

1. Galvin, J. E.; Lee, V. M.-Y.; Trojanowski, J. Q., Synucleinopathies: Clinical and Pathological Implications. *Archives of Neurology* **2001,** *58* (2), 186-190.
2. Goedert, M.; Jakes, R.; Spillantini, M. G., The Synucleinopathies: Twenty Years On. *J Parkinsons Dis* **2017,** *7*, S51-S69.
3. McCann, H.; Stevens, C. H.; Cartwright, H.; Halliday, G. M., α-Synucleinopathy phenotypes. *Parkinsonism & Related Disorders* **2014,** *20*, S62-S67.
4. Stefanis, L., α-Synuclein in Parkinson's disease. *Cold Spring Harbor perspectives in medicine* **2012,** *2* (2), a009399-a009399.
5. Kalia, L. V.; Kalia, S. K.; McLean, P. J.; Lozano, A. M.; Lang, A. E., alpha-Synuclein oligomers and clinical implications for Parkinson disease. *Ann Neurol* **2013,** *73* (2), 155-69.
6. Winner, B.; Jappelli, R.; Maji, S. K.; Desplats, P. A.; Boyer, L.; Aigner, S.; Hetzer, C.; Loher, T.; Vilar, M.; Campioni, S.; Tzitzilonis, C.; Soragni, A.; Jessberger, S.; Mira, H.; Consiglio, A.; Pham, E.; Masliah, E.; Gage, F. H.; Riek, R., In vivo demonstration that alpha-synuclein oligomers are toxic. *Proc. Natl. Acad. Sci.* **2011,** *108* (10), 4194-9.
7. Martin, Z. S.; Neugebauer, V.; Dineley, K. T.; Kayed, R.; Zhang, W.; Reese, L. C.; Taglialatela, G., α-Synuclein oligomers oppose long-term potentiation and impair memory through a calcineurin-dependent mechanism: relevance to human synucleopathic diseases. *J Neurochem.* **2012,** *120* (3), 440-452.
8. van Diggelen, F.; Hrle, D.; Apetri, M.; Christiansen, G.; Rammes, G.; Tepper, A.; Otzen, D. E., Two conformationally distinct α-synuclein oligomers share common epitopes and the ability to impair long-term potentiation. *PLoS One* **2019,** *14* (3), e0213663.
9. Emin, D.; Zhang, Y. P.; Lobanova, E.; Miller, A.; Li, X.; Xia, Z.; Dakin, H.; Sideris, D. I.; Lam, J. Y. L.; Ranasinghe, R. T.; Kouli, A.; Zhao, Y.; De, S.; Knowles, T. P. J.; Vendruscolo, M.; Ruggeri, F. S.; Aigbirhio, F. I.; Williams-Gray, C. H.; Klenerman, D., Small soluble α-synuclein aggregates are the toxic species in Parkinson's disease. *Nat. Comm.* **2022,** *13* (1), 5512.

10. Colla, E.; Jensen, P. H.; Pletnikova, O.; Troncoso, J. C.; Glabe, C.; Lee, M. K., Accumulation of Toxic α-Synuclein Oligomer within Endoplasmic Reticulum Occurs in α-Synucleinopathy In Vivo. *J. Neurosci.* **2012,** *32* (10), 3301-3305.
11. Prots, I.; Grosch, J.; Brazdis, R.-M.; Simmnacher, K.; Veber, V.; Havlicek, S.; Hannappel, C.; Krach, F.; Krumbiegel, M.; Schütz, O.; Reis, A.; Wrasidlo, W.; Galasko, D. R.; Groemer, T. W.; Masliah, E.; Schlötzer-Schrehardt, U.; Xiang, W.; Winkler, J.; Winner, B., α-Synuclein oligomers induce early axonal dysfunction in human iPSC-based models of synucleinopathies. *Proc. Natl. Acad. Sci*. **2018,** *115* (30), 7813-7818.
12. Breydo, L.; Wu, J. W.; Uversky, V. N., α-Synuclein misfolding and Parkinson's disease. *Biochimica et Biophysica Acta (BBA)-Molecular Basis of Disease* **2012,** *1822* (2), 261-285.
13. Tokuda, T.; Qureshi, M. M.; Ardah, M. T.; Varghese, S.; Shehab, S. A.; Kasai, T.; Ishigami, N.; Tamaoka, A.; Nakagawa, M.; El-Agnaf, O. M., Detection of elevated levels of alpha-synuclein oligomers in CSF from patients with Parkinson disease. *Neurology* **2010,** *75* (20), 1766-72.
14. Hansson, O.; Hall, S.; Ohrfelt, A.; Zetterberg, H.; Blennow, K.; Minthon, L.; Nagga, K.; Londos, E.; Varghese, S.; Majbour, N. K.; Al-Hayani, A.; El-Agnaf, O. M., Levels of cerebrospinal fluid alpha-synuclein oligomers are increased in Parkinson's disease with dementia and dementia with Lewy bodies compared to Alzheimer's disease. *Alzheimer's Res. Ther.* **2014,** *6* (3), 25.
15. Ugalde, C. L.; Lawson, V. A.; Finkelstein, D. I.; Hill, A. F., The role of lipids in α-synuclein misfolding and neurotoxicity. *J Biol. Chem.* **2019,** *294* (23), 9016-9028.
16. Iyer, A.; Claessens, M. M. A. E., Disruptive membrane interactions of alpha-synuclein aggregates. *Biochimica et Biophysica Acta (BBA)-Proteins and Proteomics* **2019,** *1867* (5), 468-482.
17. Fusco, G.; Chen, S. W.; Williamson, P. T. F.; Cascella, R.; Perni, M.; Jarvis, J. A.; Cecchi, C.; Vendruscolo, M.; Chiti, F.; Cremades, N.; Ying, L.; Dobson, C. M.; De Simone, A., Structural basis of membrane disruption and cellular toxicity by α-synuclein oligomers. *Science* **2017,** *358* (6369), 1440-1443.
18. Celej, María S.; Sarroukh, R.; Goormaghtigh, E.; Fidelio, Gerardo D.; Ruysschaert, J.-M.; Raussens, V., Toxic prefibrillar α-synuclein amyloid oligomers adopt a distinctive antiparallel β-sheet structure. *Biochemical Journal* **2012,** *443* (3), 719-726.
19. González-Lizárraga, F.; Socías, S. B.; Ávila, C. L.; Torres-Bugeau, C. M.; Barbosa, L. R. S.; Binolfi, A.; Sepúlveda-Díaz, J. E.; Del-Bel, E.; Fernandez, C. O.; Papy-Garcia, D.; Itri, R.; Raisman-Vozari, R.; Chehín, R. N., Repurposing doxycycline for synucleinopathies: remodelling of α-synuclein

oligomers towards non-toxic parallel beta-sheet structured species. *Scientific Reports* **2017,** *7* (1), 41755.

20. Chen, S. W.; Drakulic, S.; Deas, E.; Ouberai, M.; Aprile, F. A.; Arranz, R.; Ness, S.; Roodveldt, C.; Guilliams, T.; De-Genst, E. J.; Klenerman, D.; Wood, N. W.; Knowles, T. P. J.; Alfonso, C.; Rivas, G.; Abramov, A. Y.; Valpuesta, J. M.; Dobson, C. M.; Cremades, N., Structural characterization of toxic oligomers that are kinetically trapped during α-synuclein fibril formation. *Proc. Natl. Acad. Sci.* **2015,** *112* (16), E1994-E2003.
21. Cremades, N.; Cohen, S. I. A.; Deas, E.; Abramov, A. Y.; Chen, A. Y.; Orte, A.; Sandal, M.; Clarke, R. W.; Dunne, P.; Aprile, F. A.; Bertoncini, C. W.; Wood, N. W.; Knowles, T. P. J.; Dobson, C. M.; Klenerman, D., Direct observation of the interconversion of normal and toxic forms of α-synuclein. *Cell* **2012,** *149* (5), 1048-1059.
22. Kiechle, M.; von Einem, B.; Höfs, L.; Voehringer, P.; Grozdanov, V.; Markx, D.; Parlato, R.; Wiesner, D.; Mayer, B.; Sakk, O.; Baumann, B.; Lukassen, S.; Liss, B.; Ekici, A. B.; Ludolph, A. C.; Walther, P.; Ferger, B.; McLean, P. J.; Falkenburger, B. H.; Weishaupt, J. H.; Danzer, K. M., In Vivo Protein Complementation Demonstrates Presynaptic α-Synuclein Oligomerization and Age-Dependent Accumulation of 8–16-mer Oligomer Species. *Cell Reports* **2019,** *29* (9), 2862-2874.e9.
23. Lorenzen, N.; Nielsen, S. B.; Buell, A. K.; Kaspersen, J. D.; Arosio, P.; Vad, B. S.; Paslawski, W.; Christiansen, G.; Valnickova-Hansen, Z.; Andreasen, M.; Enghild, J. J.; Pedersen, J. S.; Dobson, C. M.; Knowles, T. P. J.; Otzen, D. E., The Role of Stable α-Synuclein Oligomers in the Molecular Events Underlying Amyloid Formation. *J. Am. Chem. Soc.* **2014,** *136* (10), 3859-3868.
24. Danzer, K. M.; Ruf, W. P.; Putcha, P.; Joyner, D.; Hashimoto, T.; Glabe, C.; Hyman, B. T.; McLean, P. J., Heat-shock protein 70 modulates toxic extracellular α-synuclein oligomers and rescues trans-synaptic toxicity. *FASEB J.* **2011,** *25* (1), 326-336.
25. Wägele, J.; De Sio, S.; Voigt, B.; Balbach, J.; Ott, M., How Fluorescent Tags Modify Oligomer Size Distributions of the Alzheimer Peptide. *Biophysical Journal* **2019,** *116* (2), 227-238.
26. Zhang, S.; Fox, D. M.; Urbanc, B., Elucidating the Role of Hydroxylated Phenylalanine in the Formation and Structure of Cross-Linked Aβ Oligomers. *J. Phys. Chem. B* **2019,** *123* (5), 1068-1084.
27. Arter, W. E.; Xu, C. K.; Castellana-Cruz, M.; Herling, T. W.; Krainer, G.; Saar, K. L.; Kumita, J. R.; Dobson, C. M.; Knowles, T. P. J., Rapid Structural, Kinetic, and Immunochemical Analysis of Alpha-Synuclein Oligomers in Solution. *Nano Letters* **2020,** *20* (11), 8163-8169.

28. Zijlstra, N.; Blum, C.; Segers-Nolten, I. M. J.; Claessens, M. M. A. E.; Subramaniam, V., Molecular Composition of Sub-stoichiometrically Labeled α-Synuclein Oligomers Determined by Single-Molecule Photobleaching. *Angewandte Chemie International Edition* **2012,** *51* (35), 8821-8824.
29. El-Agnaf, O. M. A.; Salem, S. A.; Paleologou, K. E.; Curran, M. D.; Gibson, M. J.; Court, J. A.; Schlossmacher, M. G.; Allsop, D., Detection of oligomeric forms of α-synuclein protein in human plasma as a potential biomarker for Parkinson's disease. *FASEB J.* **2006,** *20* (3), 419-425.
30. Hansson, O.; Hall, S.; Öhrfelt, A.; Zetterberg, H.; Blennow, K.; Minthon, L.; Nägga, K.; Londos, E.; Varghese, S.; Majbour, N. K.; Al-Hayani, A.; El-Agnaf, O. M. A., Levels of cerebrospinal fluid α-synuclein oligomers are increased in Parkinson's disease with dementia and dementia with Lewy bodies compared to Alzheimer's disease. *Alzheimer's Res. Ther.* **2014,** *6* (3), 25.
31. Lassen, L. B.; Gregersen, E.; Isager, A. K.; Betzer, C.; Kofoed, R. H.; Jensen, P. H., ELISA method to detect α-synuclein oligomers in cell and animal models. *PLoS One* **2018,** *13* (4), e0196056.
32. Tokuda, T.; Qureshi, M. M.; Ardah, M. T.; Varghese, S.; Shehab, S. A. S.; Kasai, T.; Ishigami, N.; Tamaoka, A.; Nakagawa, M.; El-Agnaf, O. M. A., Detection of elevated levels of α-synuclein oligomers in CSF from patients with Parkinson disease. *Neurology.* **2010,** *75* (20), 1766-1770.
33. Kumar, S. T.; Jagannath, S.; Francois, C.; Vanderstichele, H.; Stoops, E.; Lashuel, H. A., How specific are the conformation-specific α-synuclein antibodies? Characterization and validation of 16 α-synuclein conformation-specific antibodies using well-characterized preparations of α-synuclein monomers, fibrils and oligomers with distinct structures and morphology. *Neurobiology of Disease* **2020,** *146*, 105086.
34. Kulenkampff, K.; Wolf Perez, A.-M.; Sormanni, P.; Habchi, J.; Vendruscolo, M., Quantifying misfolded protein oligomers as drug targets and biomarkers in Alzheimer and Parkinson diseases. *Nat. Rev. Chem.* **2021,** *5* (4), 277-294.
35. Blömeke, L.; Pils, M.; Kraemer-Schulien, V.; Dybala, A.; Schaffrath, A.; Kulawik, A.; Rehn, F.; Cousin, A.; Nischwitz, V.; Willbold, J.; Zack, R.; Tropea, T. F.; Bujnicki, T.; Tamgüney, G.; Weintraub, D.; Irwin, D.; Grossman, M.; Wolk, D. A.; Trojanowski, J. Q.; Bannach, O.; Chen-Plotkin, A.; Willbold, D., Quantitative detection of α-Synuclein and Tau oligomers and other aggregates by digital single particle counting. *npj Parkinson's Disease* **2022,** *8* (1), 68.
36. Wang, H. Y.; Gu, Z.; Cao, C.; Wang, J.; Long, Y. T., Analysis of a single alpha-synuclein fibrillation by the interaction with a protein nanopore. *Anal Chem* **2013,** *85* (17), 8254-61.

37. Li, X.; Tong, X.; Lu, W.; Yu, D.; Diao, J.; Zhao, Q., Label-free detection of early oligomerization of α-synuclein and its mutants A30P/E46K through solid-state nanopores. *Nanoscale* **2019,** *11* (13), 6480-6488.
38. Giamblanco, N.; Fichou, Y.; Janot, J.-M.; Balanzat, E.; Han, S.; Balme, S., Mechanisms of Heparin-Induced Tau Aggregation Revealed by a Single Nanopore. *ACS Sensors* **2020,** *5* (4), 1158-1167.
39. Yu, R.-J.; Lu, S.-M.; Xu, S.-W.; Li, Y.-J.; Xu, Q.; Ying, Y.-L.; Long, Y.-T., Single molecule sensing of amyloid-β aggregation by confined glass nanopores. *Chem. Sci.* **2019,** *10* (46), 10728-10732.
40. Hu, R.; Diao, J.; Li, J.; Tang, Z.; Li, X.; Leitz, J.; Long, J.; Liu, J.; Yu, D.; Zhao, Q., Intrinsic and membrane-facilitated α-synuclein oligomerization revealed by label-free detection through solid-state nanopores. *Sci. Rep.* **2016,** *6*, 20776.
41. Abrao-Nemeir, I.; Bentin, J.; Meyer, N.; Janot, J.-M.; Torrent, J.; Picaud, F.; Balme, S., Investigation of α-Synuclein and Amyloid-β(42)-E22Δ Oligomers Using SiN Nanopore Functionalized with L-Dopa. *Chem Asian J.* **2022,** *17* (20), e202200726.
42. Meyer, N.; Janot, J.-M.; Torrent, J.; Balme, S., Real-Time Fast Amyloid Seeding and Translocation of α-Synuclein with a Nanopipette. *ACS Central Science* **2022,** *8* (4), 441-448.
43. Yusko, E. C.; Johnson, J. M.; Majd, S.; Prangkio, P.; Rollings, R. C.; Li, J.; Yang, J.; Mayer, M., Controlling protein translocation through nanopores with bio-inspired fluid walls. *Nat. Nanotech.* **2011,** *6*, 253.
44. Houghtaling, J.; List, J.; Mayer, M., Nanopore-Based, Rapid Characterization of Individual Amyloid Particles in Solution: Concepts, Challenges, and Prospects. *Small* **2018,** *14* (46), 1802412.
45. Yusko, E. C.; Prangkio, P.; Sept, D.; Rollings, R. C.; Li, J.; Mayer, M., Single-Particle Characterization of Aβ Oligomers in Solution. *ACS Nano* **2012,** *6* (7), 5909-5919.
46. Prangkio, P.; Yusko, E. C.; Sept, D.; Yang, J.; Mayer, M., Multivariate Analyses of Amyloid-Beta Oligomer Populations Indicate a Connection between Pore Formation and Cytotoxicity. *PLoS One* **2012,** *7* (10), e47261.
47. Yusko, E. C.; Bruhn, B. R.; Eggenberger, O. M.; Houghtaling, J.; Rollings, R. C.; Walsh, N. C.; Nandivada, S.; Pindrus, M.; Hall, A. R.; Sept, D.; Li, J.; Kalonia, D. S.; Mayer, M., Real-time shape approximation and fingerprinting of single proteins using a nanopore. *Nat. Nanotech.* **2017,** *12*, 360.
48. Houghtaling, J.; Ying, C.; Eggenberger, O. M.; Fennouri, A.; Nandivada, S.; Acharjee, M.; Li, J.; Hall, A. R.; Mayer, M., Estimation of Shape, Volume, and Dipole Moment of Individual Proteins Freely Transiting a Synthetic Nanopore. *ACS Nano* **2019,** *13* (5), 5231-5242.

49. Awasthi, S.; Sriboonpeng, P.; Ying, C.; Houghtaling, J.; Shorubalko, I.; Marion, S.; Davis, S. J.; Sola, L.; Chiari, M.; Radenovic, A.; Mayer, M., Polymer Coatings to Minimize Protein Adsorption in Solid-State Nanopores. *Small Methods* **2020,** *4* (11), 2000177.
50. Ying, C.; Houghtaling, J.; Eggenberger, O. M.; Guha, A.; Nirmalraj, P.; Awasthi, S.; Tian, J.; Mayer, M., Formation of Single Nanopores with Diameters of 20–50 nm in Silicon Nitride Membranes Using Laser-Assisted Controlled Breakdown. *ACS nano* **2018,** *12* (11), 11458-11470.
51. Uram, J. D.; Ke, K.; Mayer, M., Noise and Bandwidth of Current Recordings from Submicrometer Pores and Nanopores. *ACS Nano* **2008,** *2* (5), 857-872.
52. Kumar, S. T.; Donzelli, S.; Chiki, A.; Syed, M. M. K.; Lashuel, H. A., A simple, versatile and robust centrifugation-based filtration protocol for the isolation and quantification of α-synuclein monomers, oligomers and fibrils: Towards improving experimental reproducibility in α-synuclein research. *J Neurochem.* **2020,** *153* (1), 103-119.
53. Giehm, L.; Svergun, D. I.; Otzen, D. E.; Vestergaard, B., Low-resolution structure of a vesicle disrupting α-synuclein oligomer that accumulates during fibrillation. *Proc. Natl. Acad. Sci.* **2011,** *108* (8), 3246-3251.
54. Näsström, T.; Fagerqvist, T.; Barbu, M.; Karlsson, M.; Nikolajeff, F.; Kasrayan, A.; Ekberg, M.; Lannfelt, L.; Ingelsson, M.; Bergström, J., The lipid peroxidation products 4-oxo-2-nonenal and 4-hydroxy-2-nonenal promote the formation of α-synuclein oligomers with distinct biochemical, morphological, and functional properties. *Free Radic. Biol. Med.* **2011,** *50* (3), 428-437.
55. Sonn-Segev, A.; Belacic, K.; Bodrug, T.; Young, G.; VanderLinden, R. T.; Schulman, B. A.; Schimpf, J.; Friedrich, T.; Dip, P. V.; Schwartz, T. U.; Bauer, B.; Peters, J.-M.; Struwe, W. B.; Benesch, J. L. P.; Brown, N. G.; Haselbach, D.; Kukura, P., Quantifying the heterogeneity of macromolecular machines by mass photometry. *Nat. Comm.* **2020,** *11* (1), 1772.
56. Young, G.; Hundt, N.; Cole, D.; Fineberg, A.; Andrecka, J.; Tyler, A.; Olerinyova, A.; Ansari, A.; Marklund, E. G.; Collier, M. P.; Chandler, S. A.; Tkachenko, O.; Allen, J.; Crispin, M.; Billington, N.; Takagi, Y.; Sellers, J. R.; Eichmann, C.; Selenko, P.; Frey, L.; Riek, R.; Galpin, M. R.; Struwe, W. B.; Benesch, J. L. P.; Kukura, P., Quantitative mass imaging of single biological macromolecules. *Science* **2018,** *360* (6387), 423-427.
57. Stefanovic, A. N. D.; Lindhoud, S.; Semerdzhiev, S. A.; Claessens, M. M. A. E.; Subramaniam, V., Oligomers of Parkinson's Disease-Related α-Synuclein Mutants Have Similar Structures but Distinctive Membrane Permeabilization Properties. *Biochemistry* **2015,** *54* (20), 3142-3150.

58. Pieri, L.; Madiona, K.; Melki, R., Structural and functional properties of prefibrillar α-synuclein oligomers. *Sci. Rep.* **2016,** *6* (1), 24526.
59. Conway, K. A.; Lee, S.-J.; Rochet, J.-C.; Ding, T. T.; Williamson, R. E.; Lansbury, P. T., Acceleration of oligomerization, not fibrillization, is a shared property of both α-synuclein mutations linked to early-onset Parkinson's disease: Implications for pathogenesis and therapy. *Proc. Natl. Acad. Sci.* **2000,** *97* (2), 571-576.
60. Kim, H.-Y.; Cho, M.-K.; Kumar, A.; Maier, E.; Siebenhaar, C.; Becker, S.; Fernandez, C. O.; Lashuel, H. A.; Benz, R.; Lange, A.; Zweckstetter, M., Structural Properties of Pore-Forming Oligomers of α-Synuclein. *J. Am. Chem. Soc.* **2009,** *131* (47), 17482-17489.
61. Lashuel, H. A.; Petre, B. M.; Wall, J.; Simon, M.; Nowak, R. J.; Walz, T.; Lansbury, P. T., α-Synuclein, Especially the Parkinson's Disease-associated Mutants, Forms Pore-like Annular and Tubular Protofibrils. *J. Mol. Biol.* **2002,** *322* (5), 1089-1102.
62. van Diggelen, F.; Tepper, A. W. J. W.; Apetri, M. M.; Otzen, D. E., α-Synuclein Oligomers: A Study in Diversity. *Isr. J. Chem.* **2017,** *57* (7-8), 699-723.
63. Nazarian, R.; Lee, E.; Siegel, B.; Kuo, C.; Acharya, S.; Schmidt, J., Quantitative Measurements of Protein Volume and Concentration using Hydrogel-Backed Nanopores. *ACS Sensors* **2021,** *6* (3), 722-726.
64. Majbour, N. K.; Vaikath, N. N.; van Dijk, K. D.; Ardah, M. T.; Varghese, S.; Vesterager, L. B.; Montezinho, L. P.; Poole, S.; Safieh-Garabedian, B.; Tokuda, T.; Teunissen, C. E.; Berendse, H. W.; van de Berg, W. D. J.; El-Agnaf, O. M. A., Oligomeric and phosphorylated alpha-synuclein as potential CSF biomarkers for Parkinson’s disease. *Mol. Neurodegener.* **2016,** *11* (1), 7.
65. Wang, X.; Yu, S.; Li, F.; Feng, T., Detection of α-synuclein oligomers in red blood cells as a potential biomarker of Parkinson’s disease. *Neurosci. Lett.* **2015,** *599*, 115-119.
66. Li, J.; Stein, D.; McMullan, C.; Branton, D.; Aziz, M. J.; Golovchenko, J. A., Ion-beam sculpting at nanometre length scales. *Nature* **2001,** *412* (6843), 166-169.
67. Schneider, C. A.; Rasband, W. S.; Eliceiri, K. W., NIH Image to ImageJ: 25 years of image analysis. *Nat. Methods* **2012,** *9* (7), 671-675.

—Supporting Information—

Simultaneous Determination of Size and Shape of Single α-Synuclein Oligomers in Solution

Saurabh Awasthi[1*], Cuifeng Ying[1], Jiali Li[2], Michael Mayer[1*]

[1] Adolphe Merkle Institute, University of Fribourg, Chemin des Verdiers 4, CH-1700 Fribourg, Switzerland

[2] University of Arkansas, Fayetteville, AR, United States

*Corresponding Author Email ID: saurabh.awasthi@unifr.ch, michael.mayer@unifr.ch

Supplementary Note 1: *Monomer volume of α-Synuclein*

We determined the volume of αSyn monomers in solution using polymer-coated solid-state nanopores. **Supplementary Figure S1C** shows the volume estimates of αSyn monomers based on three different independent measurements revealing median volumes ranging from 32 nm^3 to 39 nm^3. These volume estimates are close to a volume of αSyn monomers of ~30 nm^3 as determined by SAXS.[S1] Moreover, we also the web server 3V[S2] for the assessment of protein volumes using two different three-dimensional structures of αSyn 1XQ8 and 2KKW determined by nuclear magnetic resonance. This approach revealed a volume of ~24 nm^3. To determine the size of αSyn oligomers, we used the mean αSyn monomer volume of 35 nm^3 determined from nanopore-based measurements. The size of αSyn oligomers estimated by nanopores ranges from dimers to 150-mers,

dimers to 175-mers, or trimers to 218-mers depending if we employed monomer volumes of 35 nm^3, 30 nm^3, or 24 nm^3, respectively for the calculation. The oligomer size range from dimers to 150-mers that we determined based on an αSyn monomer volume of 35 nm^3 agrees well with previous reports.[S3, S4]

Supplementary Note 2: *Stability of oligomers during nanopore recordings*

In order to test the stability of αSyn oligomers with respect to their size distribution in the recording conditions of nanopores (i. e. 10 mM HEPES, 2 M KCl), we incubated oligomers in PBS or in recording buffer (containing 2 M KCl) for 1 h at room temperature. Thereafter, we determined the oligomer size distribution by TEM imaging of both preparations. **Supplementary Figure S2** reveals no significant difference in the oligomer sizes for αSyn oligomers incubated for 1 h in PBS or in 2 M KCl. In addition to TEM analysis, we also used single-particle mass analysis by mass photometry to determine the effect of recording conditions on the size of oligomers. **Supplementary Figure S3 reveals** no significant difference in oligomer mass distribution was evident among oligomer samples incubated for 90 min or overnight in PBS and 2 M KCl at room temperature. Although we did not observe significant changes in oligomer size distribution in the case of αSyn oligomers studied here, recording conditions may need to be optimized for other amyloid-forming proteins.

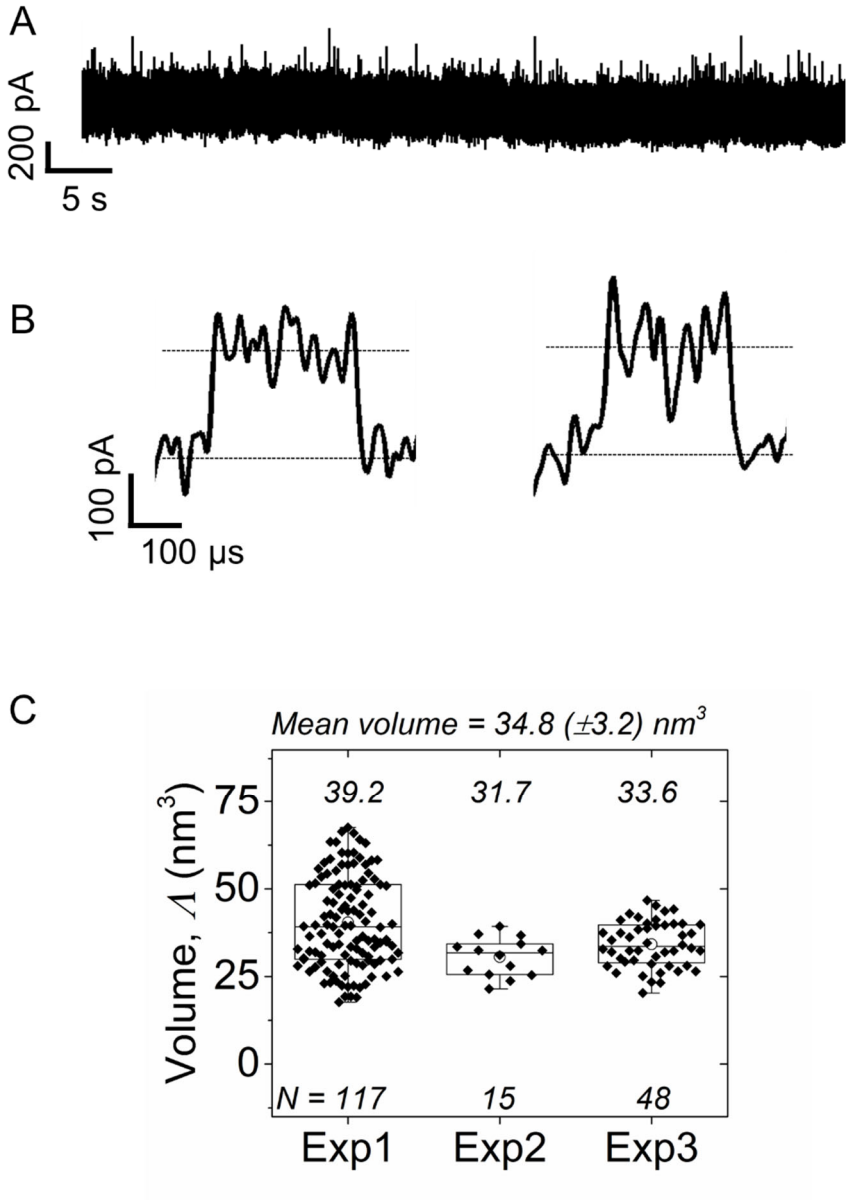

Supplementary Figure S1. Size of α-Synuclein monomers estimated by resistive pulse sensing. A. Original current trace showing individual translocation events of α-synuclein monomers through a nanopore as upward spikes. **B.** Representative individual translocation events of αSyn monomers. **C.** Volume estimates of αSyn monomer from three different nanopore experiments. These results reveal a mean volume of 34.8 (±3.2) nm^3. The diamonds show parameter estimates from intraevent analysis with horizontal lines in the box representing the median and quartile values. The mean value is shown as an open circle for each data set, with the whiskers spanning from the 10th to the 90th percentile. The median values for each data set are shown at the top of the corresponding box plot.

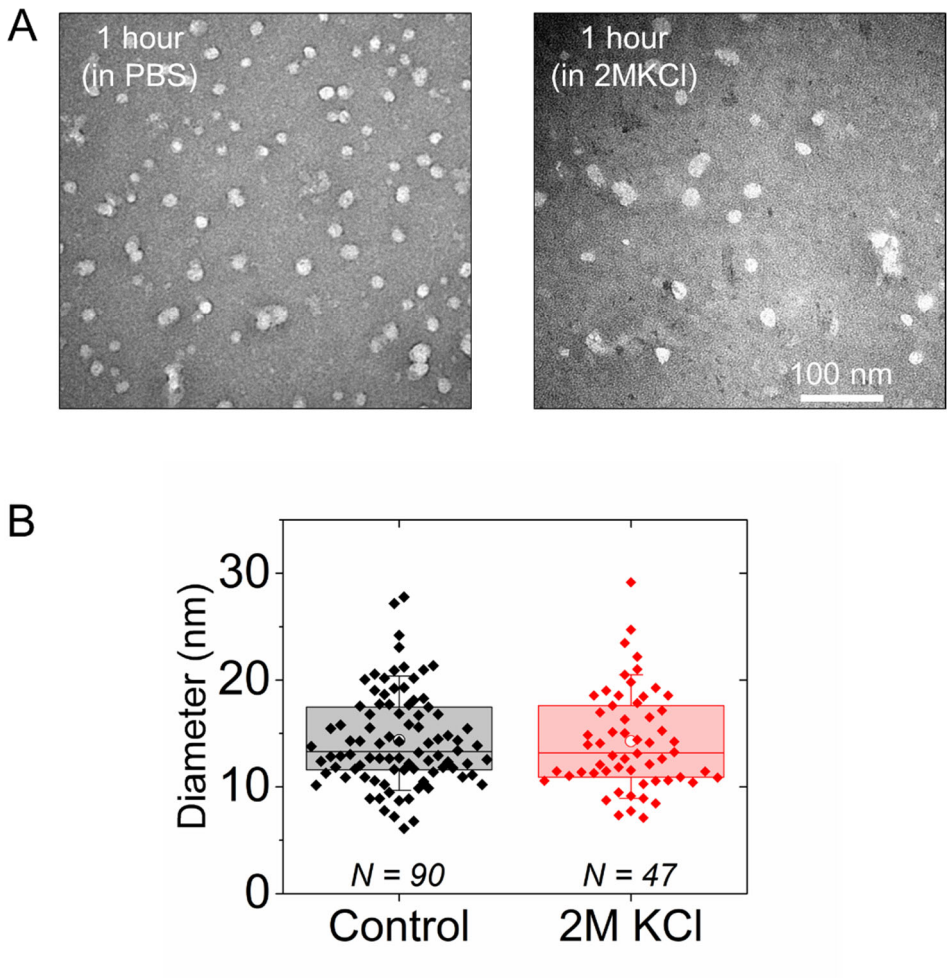

Supplementary Figure S2. Effect of recording buffer on the size of oligomers determined by TEM imaging. A. TEM micrographs of αSynuclein oligomers after 1 h of incubation in PBS (control) or in nanopore recording buffer (i.e. 2 M KCl). **B.** Comparative analysis of oligomer size distribution after incubation in PBS buffer or in 2 M KCl. The diamonds show estimates of oligomer diameter from size analysis of single particles with horizontal lines in the box representing the median and quartile values. The mean value is shown as an open circle for each data set, with the whiskers spanning from the 10th to the 90th percentile. No significant change in oligomer sizes occurred within 1 h of incubation in 2 M KCl.

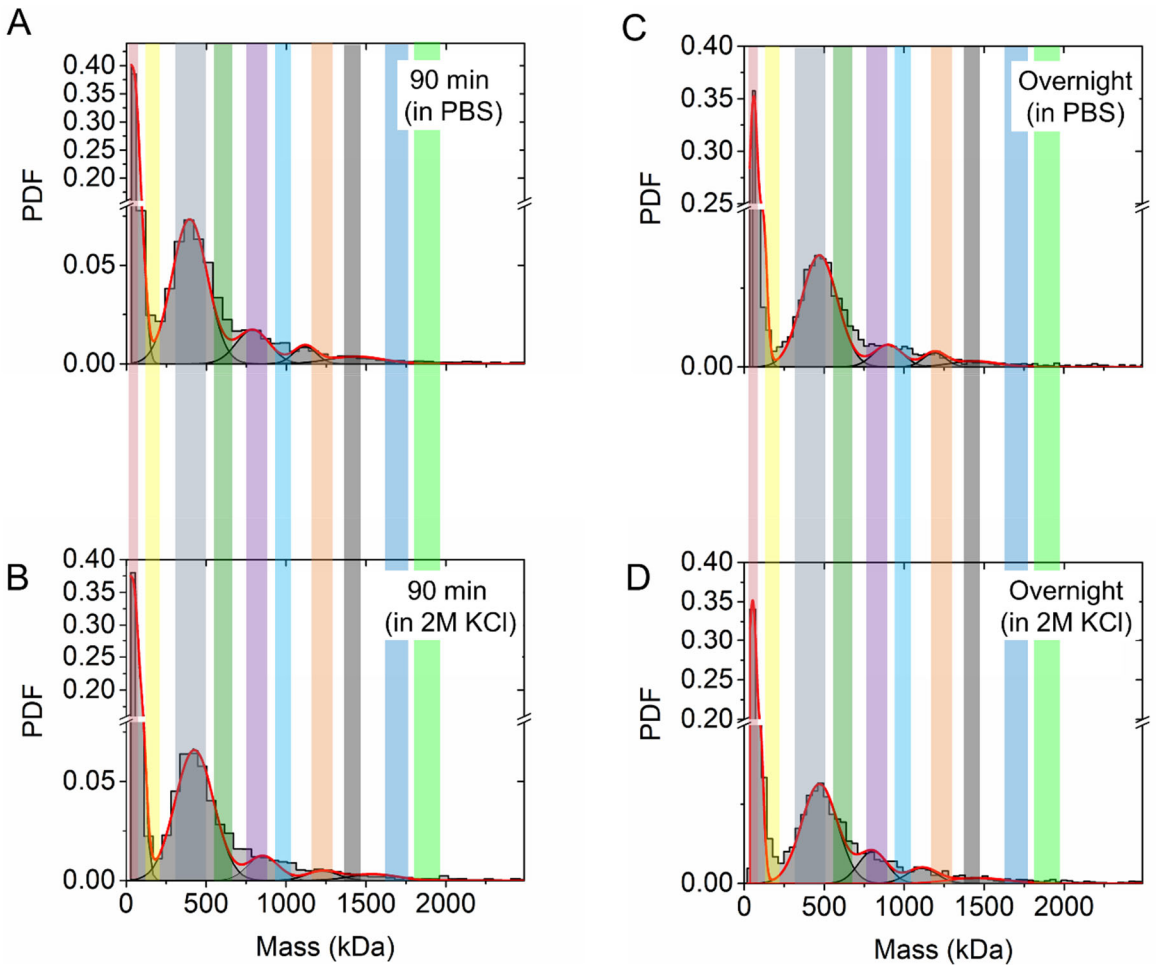

Supplementary Figure S3. Effect of recording buffer on oligomer size distribution determined by mass photometry. A. Size distribution of α-Synuclein oligomers after 90 min incubation in PBS. **B.** Size distribution of α-Synuclein oligomers after 90 min incubation in 2 M KCl. **C.** Size distribution of α-Synuclein oligomers after overnight incubation in PBS. **D.** Size distribution of α-Synuclein oligomers after overnight incubation in 2 M KCl. For comparison, the shaded regions in different colors show the presence/absence of different oligomer populations in different conditions.

References (SI)

S1. Giehm, L.; Svergun, D. I.; Otzen, D. E.; Vestergaard, B., Low-resolution structure of a vesicle disrupting α-synuclein oligomer that accumulates during fibrillation. *Proc. Natl. Acad. Sci. U. S. A.* **2011,** *108* (8), 3246-3251.

S2. Voss, N. R.; Gerstein, M., 3V: cavity, channel and cleft volume calculator and extractor. *Nucleic Acids Res.* **2010**, 38 (suppl_2), W555-W562.

S2. Cremades, N.; Cohen, S. I. A.; Deas, E.; Abramov, A. Y.; Chen, A. Y.; Orte, A.; Sandal, M.; Clarke, R. W.; Dunne, P.; Aprile, F. A.; Bertoncini, C. W.; Wood, N. W.; Knowles, T. P. J.; Dobson, C. M.; Klenerman, D., Direct observation of the interconversion of normal and toxic forms of α-synuclein. *Cell* **2012,** *149* (5), 1048-1059.

S3. Nässtrom, T.; Fagerqvist, T.; Barbu, M.; Karlsson, M.; Nikolajeff, F.; Kasrayan, A.; Ekberg, M.; Lannfelt, L.; Ingelsson, M.; Bergström, J., The lipid peroxidation products 4-oxo-2-nonenal and 4-hydroxy-2-nonenal promote the formation of α-synuclein oligomers with distinct biochemical, morphological, and functional properties. *Free Radic. Biol. Med.* **2011,** *50* (3), 428-437.